

## ***Supporting Information***

### Exploration of One-Dimensional Iron-Based Coordination Polymer for Enhanced Lithium Storage Capabilities

Jingwei Liu<sup>1</sup>, Xiaolong Cheng<sup>1</sup>, Shifa Dang<sup>1</sup>, Weile Kong<sup>2</sup>, Mengxian Zheng<sup>1</sup>, Lei Zhang<sup>1</sup>, Shuangyan Wu<sup>2\*</sup>, Ning Liu<sup>3\*</sup>, Jinchao Cao<sup>4\*</sup>

1. Hebei Key Laboratory of Low Carbon and High Efficiency Power Generation Technology, North China Electric Power University, Baoding 071003, Hebei, China.
2. Key Laboratory of Inorganic Molecule-Based Chemistry of Liaoning Province and Laboratory of Coordination Chemistry, Shenyang University of Chemical Technology, Shenyang, 110142, China.
3. Key Laboratory of Advanced Energy Materials Chemistry (MOE), Frontiers Science Center for New Organic Matter and State Key Laboratory of Advanced Chemical Power Sources, College of Chemistry, Nankai University, Tianjin 300071, China.
4. Binzhou Institute of Technology, Weiqiao-UCAS Science and Technology Park, Binzhou, 256606, Shandong, China.

\*Corresponding author. E-mail address: wushuangyan90@syuct.edu.cn (Shuangyan Wu); Ning Liu (1337199177@qq.com); caojinchao@wqucas.com (Jinchao Cao)

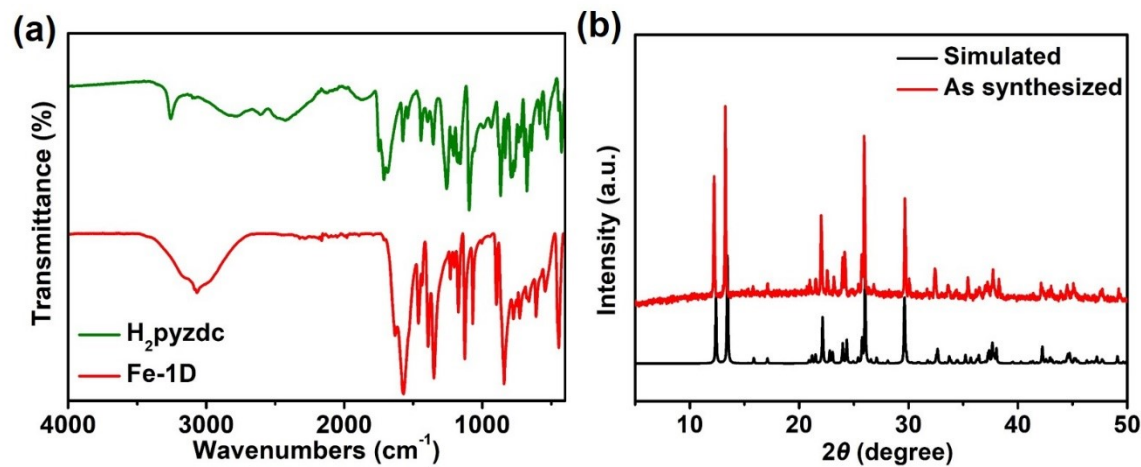


**Figure S1.** (a) Infrared spectra of Fe-1D, (b) PXRD of Fe-1D.

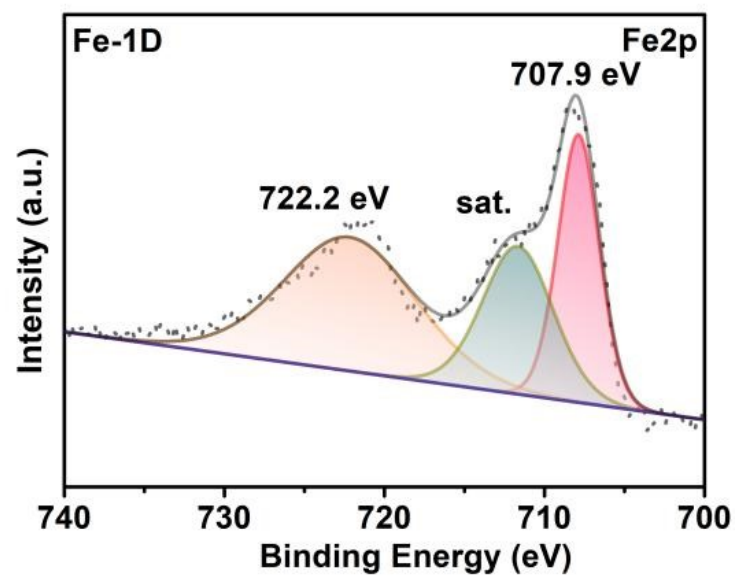


**Figure S2.** Fe 2p high-resolution XPS spectrum of Fe-1D.

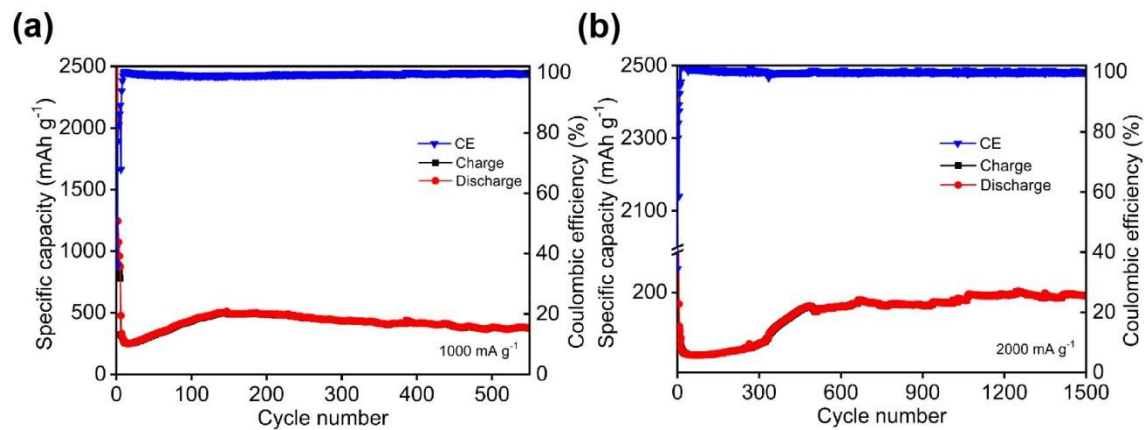


**Figure S3.** (a) Charge-discharge profiles at  $1000 \text{ mA g}^{-1}$ , (b) Charge-discharge profiles at

$2000 \text{ mA g}^{-1}$ .

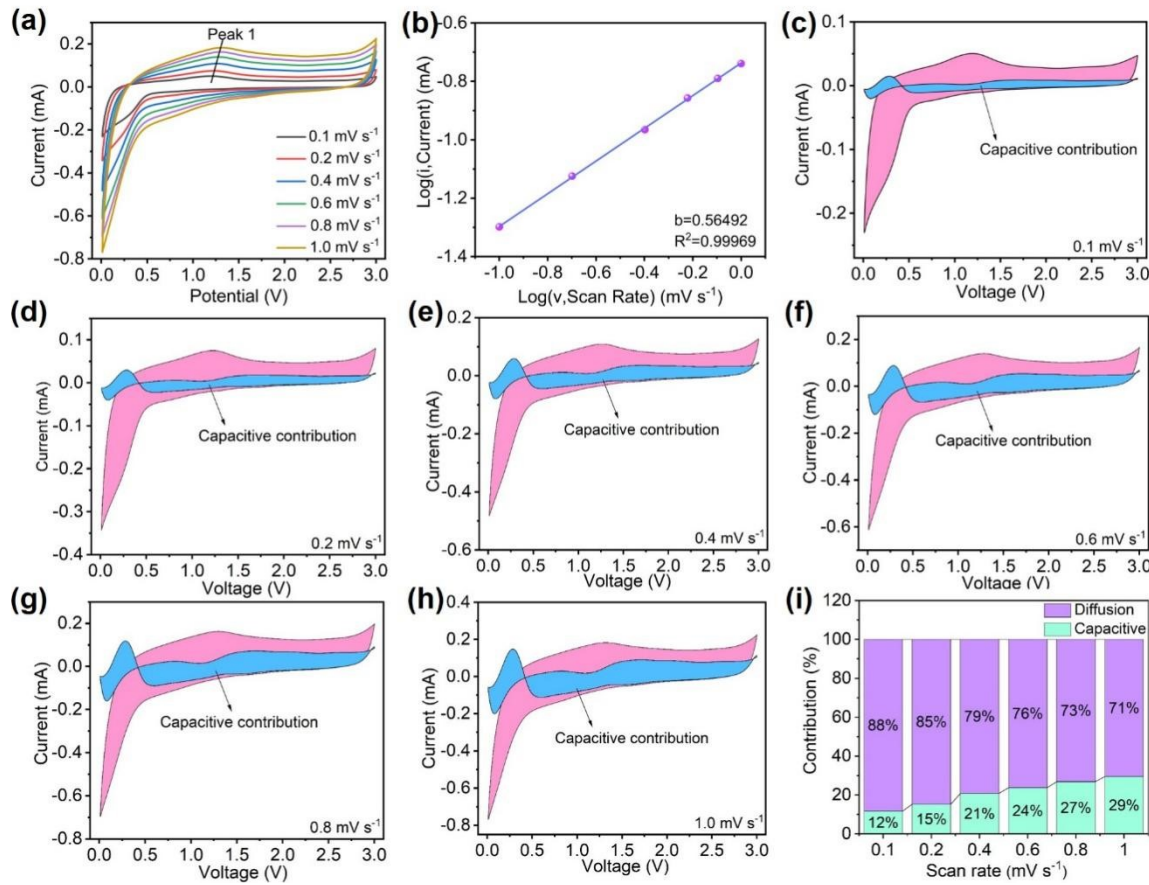


**Figure S4.** (a) CV curves at different scan rates of Fe-1D, (b) Log (i) vs log (v) plots at specific peak current of Fe-1D, (c-h) Pseudo-capacitance control contribution at 0.1, 0.2, 0.4, 0.6, 0.8, 1.0  $\text{mV}\cdot\text{s}^{-1}$  as a percentage of the total capacity contribution of Fe-1D, (i) The relative contributions of pseudocapacitive capacities and diffusion-controlled capacities at various scan rates.

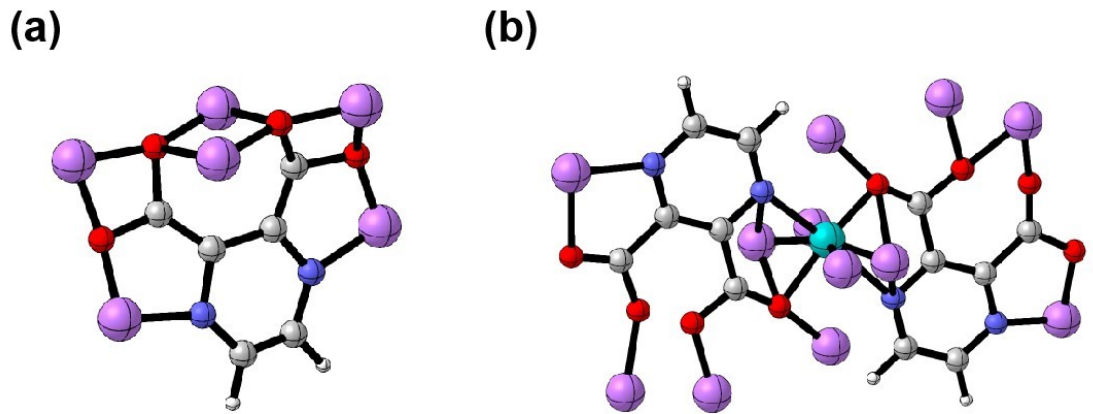


**Figure S5.** Theoretical lithium storage sites of (a) 2,3-Pyrazinedicarboxylic acid and (b) Fe-1D.

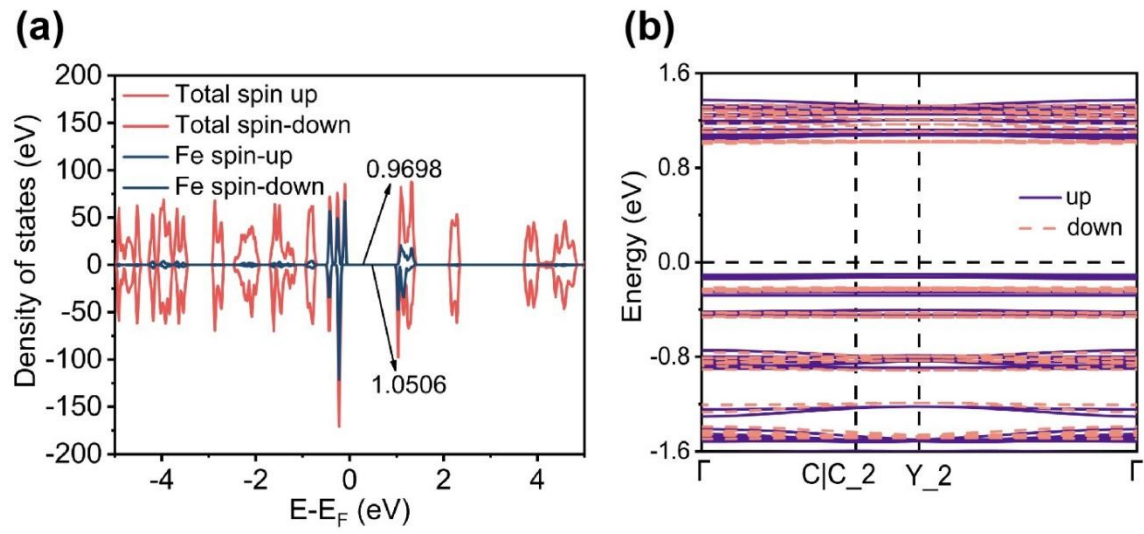


**Figure S6.** (a) Density of states (DOS) and (b) Electronic band structure of Fe-1D.

**Table S1.** Calculated theoretical capacities and LUMO/HOMO energy levels of the selected aromatic ligands

Structure						
Molecular formula	C <sub>6</sub> H <sub>6</sub> O	C <sub>7</sub> H <sub>6</sub> O	C <sub>7</sub> H <sub>6</sub> O <sub>2</sub>	C <sub>8</sub> H <sub>6</sub> O <sub>4</sub>	C <sub>7</sub> H <sub>5</sub> NO <sub>4</sub>	C <sub>6</sub> H <sub>4</sub> N <sub>2</sub> O <sub>4</sub>
Theoretical number of Li uptake	1	1	2	4	5	6
Theoretical Capacity (mAh g <sup>-1</sup> )	285	253	439	646	801	956
LUMO (Hartree)	-0.002	-0.069	-0.057	-0.069	-0.076	-0.099
HOMO (Hartree)	-0.242	-0.257	-0.265	-0.277	-0.279	-0.268
Energy level gap (eV)	6.53	5.11	5.66	5.64	5.52	<b>4.6</b>

1 Hartree = 27.211386230 eV

**Table S2.** Crystallographic data and refinement parameters

Empirical formula	C <sub>12</sub> H <sub>8</sub> FeN <sub>4</sub> O <sub>10</sub>
Formula weight	424.07
Temperature/K	298
Crystal system	monoclinic
Space group	I2/a
a/Å	14.9219(19)
b/Å	8.4923(7)
c/Å	13.0852(17)
α/°	90
β/°	118.145(17)
γ/°	90
Volume/Å <sup>3</sup>	1462.1(4)
Z	4
ρcalcg/cm <sup>3</sup>	1.927
μ/mm-1	1.104
F(000)	856
Radiation	MoKα ( $\lambda = 0.71073$ )
2θ range for data collection/°	5.71 to 52.994
Index ranges	-17 ≤ h ≤ 18, -10 ≤ k ≤ 10, -15 ≤ l ≤ 16
Reflections collected	4511
Independent reflections	1515 [R <sub>int</sub> = 0.0385, R <sub>sigma</sub> = 0.0701]
Data/restraints/parameters	1515/0/126
Goodness-of-fit on F <sup>2</sup>	1.025
Final R indexes [I>=2σ (I)]	R <sub>1</sub> = 0.0465, wR <sub>2</sub> = 0.1151
Final R indexes [all data]	R <sub>1</sub> = 0.0707, wR <sub>2</sub> = 0.1241
Largest diff. peak/hole / e Å <sup>-3</sup>	0.54/-0.53

**Table S3.** The hydrogen bond parameters

D-H···A	D-H (Å)	H···A (Å)	D···A (Å)	D-H-A (°)
O(4)-H4···O(5)	0.82	1.69	2.489	166
O(5)-H5A···O(1)	0.85	1.72	2.524	158
O(5)-H5B···N(2)	0.85	1.91	2.755	174

**Table S4.** The simulated values for impedance spectra before and after 140 cycles

Sample	R <sub>1</sub>	R <sub>2</sub>	C <sub>1</sub>	R <sub>ct</sub>	C <sub>2</sub>	W <sub>1-R</sub>	W <sub>1-T</sub>	W <sub>1-P</sub>
As assembled	4.385	63.3	7.69×10 <sup>-7</sup>	307	2.81×10 <sup>-6</sup>	36.53	0.60	0.37
After 140 cycles	10.04	12.75	6.43×10 <sup>-7</sup>	20.21	2.77×10 <sup>-5</sup>	20.39	0.43	0.37

**Table S5.** Cartesian coordinates for 2,3-Pyrazinedicarboxylic acid lithium storage.

Cartesian coordinates for H <sub>2</sub> pYZDC in lithium storage state							
Element	Coordinates			Element	Coordinates		
	X	Y	Z		X	Y	Z
C	-0.608466	-2.765617	0.209386	O	2.985352	0.660865	-0.222401
C	0.699153	-2.758312	-0.187117	C	-1.611892	0.625924	-0.243653
N	1.420167	-1.570464	-0.255792	O	-2.994979	0.462525	-0.101306
C	0.767202	-0.376939	-0.115026	O	-1.314437	2.020576	-0.405093
C	-0.715961	-0.382383	0.050323	Li	0.385661	2.340653	-0.969262
N	-1.337848	-1.625766	0.423026	Li	2.967953	1.938533	1.003171
H	-1.123887	-3.705771	0.384596	Li	-3.120411	2.208651	-0.413433
H	1.247454	-3.674345	-0.365935	Li	-0.437502	1.724761	-0.413433
C	1.563023	0.799907	-0.230478	Li	3.203638	-1.053584	-0.413433
O	1.216778	1.983109	0.632961	Li	-3.132627	-1.198476	-0.413433

**Table S6.** Cartesian coordinates for Fe-1D lithium storage.

Cartesian coordinates for Fe-1D in lithium storage state								
Element	Coordinates			Element	Coordinates			
	X	Y	Z		X	Y	Z	
C	-4.267539	0.617647	0.004618	O	-3.332715	-2.029725	-0.078487	
C	2.876032	-0.352126	0.096159	C	-5.30412	-0.540792	0.046475	
N	1.964415	-1.344018	0.160857	O	-5.137745	-1.759744	0.040299	
C	2.449187	-2.602284	0.133645	O	-6.577726	-0.079846	0.129339	
C	3.840711	-2.867823	0.042089	C	5.298484	0.524018	-0.068557	
N	4.752274	-1.875946	-0.022606	O	6.52524	0.479355	-0.150018	
H	1.711046	-3.419737	0.186068	O	4.714157	1.748277	-0.034499	
H	4.227932	-3.900023	0.020451	Fe	0.068356	-0.154514	0.028234	
C	2.335219	1.089474	0.126361	Li	-1.225114	0.099533	1.066233	
O	1.177836	1.499772	0.201739	Li	1.525839	0.181283	-0.914471	
O	3.327045	2.012957	0.056575	Li	-0.099004	-0.102382	-1.428999	
C	-2.454845	2.585531	-0.155768	Li	0.255011	0.129689	1.655052	
C	-3.846357	2.851053	-0.064227	Li	-2.617331	-3.778632	-0.119494	
N	-4.757974	1.859416	0.000471	Li	0.157802	-2.625928	-0.662981	
C	-4.273202	0.600894	-0.026741	Li	2.611648	3.761864	0.097151	
C	-2.881678	0.335356	-0.118297	Li	-0.330886	2.510181	0.129655	
N	-1.970115	1.327232	-0.182992	Li	-4.516662	-3.418516	0.524054	
H	-1.716687	3.402971	-0.208162	Li	4.869813	3.758316	0.118641	
H	-4.233577	3.883233	-0.042602	Li	6.812142	-1.608313	0.019293	
C	-2.340875	-1.106247	-0.148517	Li	-6.637758	1.777408	-0.186783	
O	-1.183495	-1.516551	-0.223908					

**Table S7.** The basic electrochemical properties of the Fe-based anode materials.

Electrode materials	Capacity (mAh g <sup>-1</sup> )	Current density (mA g <sup>-1</sup> )	Cycle number	Voltage (V)	Refs
Fe-ZIF@C	719	100	100	0.01-2.5	1
Fe <sub>3</sub> O <sub>4</sub> @C	570	100	60	0.01-3	2
[Fe(C <sub>5</sub> O <sub>5</sub> )(H <sub>2</sub> O) <sub>3</sub> ] <sub>n</sub> ( <b>1D</b> )	521	100	140	0.01-2.4	3
Ti <sub>0.9</sub> Fe <sub>1.1</sub> O <sub>3</sub>	454.9	100	500	0.01-2.5	4
Fe <sub>3</sub> O <sub>4</sub> /GN (15%)	825	100	100	0.01-3	5
MIL-88B(Fe)	189	200	100	0.1-3	6
Fe <sub>2</sub> (SO <sub>4</sub> ) <sub>3</sub>	540	1000	100	0.01-3	7
Fe <sub>3</sub> O <sub>4</sub> @CTP QDs-2	810	100	200	0.01-3	8
Fe <sub>3</sub> O <sub>4</sub>	108	100	200	0.01-3	
semi-crystalline Fe-MOF	854	85	100	0.01-3	9
Fe-1D	833	200	300	0.01-3	this work

***Theoretical methods and computational details:***

Band structure analysis and the corresponding projected density of states (PDOS) calculations for Fe-1D were conducted using the Vienna Ab initio Simulation Package (VASP).<sup>10,11</sup> For the electronic structure calculations, the Generalized Gradient Approximation (GGA) in conjunction with the Perdew-Burke-Ernzerhof (PBE) functional<sup>12</sup> was employed. The kinetic energy cut-off was set to 400 eV, and the K-point mesh was configured as 2 x 3 x 2. The optimization process was terminated when both the energy and force criteria converged to 1.0 x 10-5 eV and 0.02 eV/Å, respectively.

Calculations pertaining to HOMO/LUMO and ESP for both H2pyzdc and Fe-1D were executed using Gaussian 16 software.<sup>13</sup> Geometric optimization and frequency analysis were carried out employing the B3LYP functional, in conjunction with a hybrid basis set: SDD for Co and Ni atoms,<sup>14</sup> and 6-311+G(d)<sup>15</sup> for C, H, N, and O atoms.

**References:**

- [1] J. Nie, Z. Li, G. Shi, J. Wang, S. Yao, "Fe-ZIF@C with Porous Nanostructure as Anode Material for Lithium-Ion Batteries," *Journal of Electronic Materials* 50 (2021): 2831-2839.
- [2] J. Wang, M. Gao, H. Pan, et al., "Chemical vapor deposition prepared bi-morphological carbon-coated Fe<sub>3</sub>O<sub>4</sub> composites as anode materials for lithium-ion batteries," *Journal of Power Sources* 282 (2015): 257-264.
- [3] L. Zhang, X. Zhang, Y. Gui, "One-Dimensional Croconate-Based Fe-CP as a High-Performance Anode Material for Lithium-Ion Batteries," *Polymers* 15.18 (2023): 3728.
- [4] J. Yang, J. Hou, M. Xu, et al., "Improved cycle capability of Titanium-doped Fe<sub>2</sub>O<sub>3</sub> anode material for Li-ion batteries," *Journal of Alloys and Compounds* 722 (2017): 414-419.
- [5] J. Jiao, W. Qiu, L. Chen, et al., "Synthesis of well-defined Fe<sub>3</sub>O<sub>4</sub> nanorods/N-doped graphene for lithium-ion batteries," *Nano research* 9 (2016): 1256-1266.
- [6] D. Pukazhselvan, CM. Granadeiro, G. Gonçalves, et al., "Comparative analyses of MIL-88B (Fe) and MIL-100 (Fe) metal organic frameworks as active anode materials for Li ion batteries," *Electrochimica Acta* 465 (2023): 142989.
- [7] J. Yao, B. Huang, J. Jiang, et al., "Electrochemical performance of Fe<sub>2</sub>(SO<sub>4</sub>)<sub>3</sub> as a novel anode material for lithium-ion batteries," *Journal of Alloys and Compounds* 886 (2021): 161238.

- [8] F. Shi, Q. Liu, C. Zhang, et al., "A facile method to prepare Fe<sub>3</sub>O<sub>4</sub>@CTP QDs composite as advanced anode material for lithium ion batteries," *Journal of Alloys and Compounds* 890 (2022): 161911.
- [9] L. Moutanassim, M. Aqil, S. El. Hankari, et al., "Disordered and defective semi-crystalline Fe-MOF as a high-power and high-energy anode material for lithium-ion batteries," *Journal of Energy Storage* 93 (2024): 112055.
- [10] G. Kresse, J. Hafner, "Ab initio molecular-dynamics simulation of the liquid-metal–amorphous-semiconductor transition in germanium," *Physical Review B* 49 (1994): 14251.
- [11] G. Kresse, J. Furthmüller, "Efficiency of ab-initio total energy calculations for metals and semiconductors using a plane-wave basis set," *Computational materials science* 6 (1996): 15-50.
- [12] J. P. Perdew, K. Burke, M. Ernzerhof, "Generalized gradient approximation made simple," *Physical review letters* 77 (1996): 3865.
- [13] M. J. Frisch, G. W. Trucks, H. B. Schlegel, et al., "Gaussian 16. Revision C.01 Gaussian Inc.," *Wallingford, CT, USA. 2016.*
- [14] C. Lee, W. Yang, R. G. Parr, "Development of the Colle-Salvetti correlation-energy formula into a functional of the electron density," *Physical review B* 37 (1988): 785.
- [15] D. Andrae, U. Haeussermann, M. Dolg, et al., "Energy-adjusted ab initio pseudopotentials for the second and third row transition elements," *Theoretica chimica acta* 77 (1990): 123-141.